PCCP

PAPER

The role of pressure and defects in the wurtzite to rock salt transition in cadmium selenide†

Cite this: DOI: 10.1039/d1cp05051f

Anders Lervik, *[a] Ingeborg-Helene Svenum,[b] Zhaohui Wang,[c] Raffaela Cabriolu,[ad] Enrico Riccardi,[ae] Stefan Andersson[c] and Titus S. van Erp[a]

Received 4th November 2021,
Accepted 18th March 2022

DOI: 10.1039/d1cp05051f

rsc.li/pccp

Using molecular dynamics and path sampling techniques we investigated the effect of pressure and defects in the wurtzite to rock salt transition in cadmium selenide (CdSe). In the pressure range 2–10 GPa, rate constants of transition are in the order of 10^{-23} to 10^{5} s^{-1} for the transformation of a relatively small wurtzite crystal consisting of 1024 atoms with periodic boundary conditions. The transition paths predominantly evolve through an intermediate 5-coordinated structure, as reported before, though its typical lifetime within the transition paths is particularly long in the intermediate pressure range (4–6 GPa). The defects were created by removing Cd–Se pairs from an otherwise perfect crystal. The removals were either selected fully randomized or grouped in clusters (cavity creation). We find that the rate of transition due to the defects increases by several orders of magnitude even for a single pair removal. This is caused by a change in the transition mechanism that no longer proceeds *via* the intermediate 5-coordinated structure, when defects are present. Further, the cavity creation yields a lower rate than the fully randomized removal.

1 Introduction

The materials properties of cadmium selenide (CdSe) have been studied extensively in recent years, both experimentally and computationally, because of its promising performance as a nanostructured semiconductor material in several applications ranging from solar cells, light-emitting diodes, and biological imaging techniques.[1–3] The importance of defects, such as vacancies, for the electronic and magnetic properties of CdSe has attracted significant attention.[4–6] The pressure-induced phase transformation between the four-fold coordinated wurtzite and the six-fold coordinated rock salt structures in CdSe has been the topic of several computational studies. Nanocrystals[7–11] and nanowires[11–13] have gained the most interest, but there are also studies of the bulk CdSe materials.[14–21]

Sheppard *et al.*[14] studied the energetics of transition paths of bulk CdSe by the generalized solid-state nudged elastic band (G-SSNEB) method. The focus was on the energy profile and mechanism of the rock salt to wurtzite transition. It was demonstrated that with sufficiently large simulation cells (containing about 10^4 atoms) a local nucleation event could be described whereas only a concerted transition mechanism was allowed for small cells (about 10^2 atoms). The transition states between a multitude of CdSe polymorphs were studied by Xiao *et al.*[15] using the solid-state dimer method for optimizing saddle points on the potential energy surface and adaptive kinetic Monte Carlo simulations to explore transition paths and corresponding crystal phases. Through this approach, several previously unknown crystal phases were found. Recently, a low-energy transition pathway was discovered using swarm intelligence and graph theory.[21]

To make the transition, the system has to overcome a very high free energy barrier. Even at pressures far beyond the phase transition pressure (approximately 2–2.5 GPa,[22–24]) the timescale required to cross the barrier is not accessible by molecular dynamics (MD). Both Shimojo *et al.*[16] and Bealing *et al.*,[19] therefore, used pressurised molecular dynamics (MD) to elucidate the dynamics of the wurtzite to rock salt transition mechanisms.

Shimojo *et al.*[16] and Bealing *et al.*[19] enforced the reaction by applying a pressure ramp of 1 GPa per, respectively 2 and 50 ps (up to 11 GPa where the transition spontaneously happens in MD[19]). Different mechanisms were identified[16] among which

[a] Department of Chemistry, Norwegian University of Science and Technology, Høgskoleringen 5, 7491 Trondheim, Norway. E-mail: anders.lervik@ntnu.no
[b] Department of Materials and Nanotechnology, SINTEF Industry, P.O. Box 4760 Torgarden, 7465 Trondheim, Norway
[c] Department of Metal Production and Processing, SINTEF Industry, P.O. Box 4760 Torgarden, 7465 Trondheim, Norway
[d] Department of Physics, Norwegian University of Science and Technology, Høgskoleringen 5, 7491 Trondheim, Norway
[e] Department of Informatics, UiO, Gaustadalléen 23B, 0373 Oslo, Norway

† Electronic supplementary information (ESI) available. See DOI: 10.1039/d1cp05051f

an intermediate transition to a structure of stacked flat honeycomb lattices, which seemed to be the dominant mechanism. The rate of simulated pressure increase is, however, immense compared to the rate in standard pressure experiments.[23] The observed transitions might, therefore, not necessarily reflect the mechanism of these experiments.

Bealing *et al.*[18,19] also applied metadynamics[25] that allows the study of the transition close to the experimental phase transition pressure. Still, metadynamics relies on an adaptive process in which the underlying potential is slowly modified such that the system is lifted out of the free energy minima. This leads to artificial biasing forces that naturally disturb the true Newtonian dynamics of the system.

The transition path sampling method (TPS)[26] enables the study of rare transitions without altering the dynamics or the underlying potential energy surface. TPS is based on the sampling of many short MD trajectories that are encouraged to cross the barrier *via* a detailed-balance Monte Carlo (MC) protocol. The approach can hence be used to study the unbiased dynamics of the solid–solid transition at lower pressures. Zahn *et al.*[17] applied TPS for generating numerous transition trajectories at 2.5 GPa that were later on analysed by visual inspection. The analysis revealed that transition paths evolve according to two equiprobable reaction mechanisms. At first, a nucleation center quickly transforms into a 2D slab, which is then followed by two possible different layer-shifting steps mechanisms. In a similar study, Leoni *et al.*[20] used TPS to study the formation of defects in the form of nanodomains of wurtzite and meta-stable zinc blende structures in the transformation from the rock-salt structure. The resulting structures showed favourable agreement with experiments.

While the TPS approach provides quantitative statistical information on how the process can evolve provided that the transition is successful, it will not tell how likely it is that the actual event takes place. As a result, the single reactive path ensemble TPS approach, as conducted by Zahn *et al.*,[17] cannot compute reaction rates. In addition, it won't directly reveal what mechanistic steps or initial conditions are essential for triggering the event as this would require a statistical comparison between reactive and unreactive events with nearly identical starting conditions. Even though some analysis in this direction can be made based on the rejected moves,[27] these failed trajectories do not necessarily comprise a well-defined statistical path ensemble.

Therefore, a fully quantitative analysis of rates and reaction triggers *via* a TPS type approach requires the simulation of not just one reactive path ensemble, but a series of path ensembles. The difference between the path ensembles within the series is then the minimal progress along a reaction coordinate (also referred to as order parameter or progress coordinate) that is maintained by the MC acceptance/rejection step. In the original TPS paper,[26] the minimal progress was determined by the endpoint of the path using a fixed path length ensemble. This algorithmic approach was later on improved by the transition interface sampling (TIS)[28] and replica exchange TIS (RETIS)[29] methods where the minimal progress was translated into an interface crossing condition using a flexible path length algorithm. The different path ensembles can further be analyzed using classification schemes to understand the collective variables that have predictive power with respect to reactivity.[30–32] Still, if the reaction barrier is steep, as in the wurtzite to rock salt transitions, a large number of closely placed interfaces needs to be defined to guarantee sufficient overlap between the different path ensembles. This makes a full path ensemble evaluation that allows quantitative computation of reaction rates a challenge for this system.

This paper reports the first estimates of transition rates, calculated using the RETIS algorithm, for the wurtzite to rock salt transition. In addition to the study of transitions between perfect crystals, we also examined the effect of defects by random removal of Cd–Se pairs from the wurtzite structure. Here, both the pressure, the number of removed pairs, and the type of created cavities (either due to random uncorrelated removal or by removal in clusters) are varied to analyse their effect on the transition rate. In Section 2, we present our computational approach and the details of our molecular dynamics and rare event sampling simulations. Section 3 contains the results on the simulations of pressure-induced phase transformations, without and with defects, and our discussion of the significance of our findings. Finally, our conclusions are presented in Section 4.

2 Computational methodology

2.1 Molecular dynamics simulations

To generate initial trajectories for the rare event simulations, and to study the equilibrium structures at different pressures, we carried out equilibrium molecular dynamics (MD) simulations. The MD simulations were carried out using GROMACS[33] (versions 2019.4 and 2020.1) and the interactions were modeled using the force field of Rabani.[24] The coulombic interactions were obtained using the smooth particle mesh Ewald (PME) method[34] with a real-space cut-off of 0.9 nm, van der Waals interactions were truncated at 0.9 nm, and dispersion corrections were applied to the energy and pressure terms. Periodic boundary conditions were applied in all directions and the pressure was coupled using an anisotropic Berendsen barostat with a coupling parameter of 4 ps. The temperature was coupled to 300 K using the thermostat of Bussi *et al.*[35] with a coupling parameter of 0.5 ps. The equations of motion were integrated using the velocity Verlet algorithm with a time-step of 0.5 fs.

The thermostats of Bussi *et al.* and Berendsen are very similar in the sense that both are based on the rescaling of velocities. However, only the former samples the exact canonical distribution and is, therefore, preferred. In principle, the Berendsen barostat has the same problem of not generating the exact pressure fluctuations, but here we lacked good alternatives within the GROMACS set-up. The recently introduced barostat by Bernetti and Bussi[36] is again a similar but exact, variant of the Berendsen barostat. However, the current

implementation in GROMACS does not allow for anisotropic box changes. We also tested the Parrinello–Rahman[37] barostat that is also exact from the thermodynamics perspective. However, the dynamical behaviour showed large box oscillations. This is a known issue for this barostat when the conditions are far from equilibrium, which is typical for transition paths. We, therefore, opted for the Berendsen barostat and the Bussi thermostat as a good compromise between exactness and practicality.

To study the equilibrium structures, we created initial wurtzite and rock salt lattices consisting of 512 Cd atoms and 512 Se atoms. These initial structures were equilibrated at the target pressures (2 GPa, 4 GPa, 6 GPa, 8 GPa, 10 GPa) in short MD simulations (lasting 0.1 ns), and following this, we ran production MD simulations lasting 10 ns. From these simulations, we calculated the volume per atom, which we used to define the order parameter for the rare event simulations (see Section 2.2), and radial distribution functions, which we used to define cut-off distances for the coordination analysis (see Section 2.4). We also considered a pressure of 11 GPa, but in this case, the wurtzite structure is not stable at the typical MD time scale,[19] and will spontaneously transition into a rock salt structure in less than 30 ps. Anticipating the results from the rare event simulations, we observed seemingly stable 5-coordinated conformations (a honeycomb-like[16] or h-MgO-structure[7]) as intermediate states at the lower pressures. To study the stability of these conformations, we extracted snapshots containing honeycomb structures and subjected them to equilibrium MD simulations using the same protocol as for the wurtzite/rock salt structures. Representative snapshots of the different structures are given in Fig. 1.

To generate initial trajectories for the rare event simulations (see Section 2.2) we performed MD simulations as follows: for each pressure, we first transformed the initial wurtzite structure to a rock salt structure by applying a continuous strain (using LAMMPS[38] with interaction parameters identical to the ones used above, but without temperature and pressure coupling). From each of these trajectories, we extracted 100 frames along the deformation trajectory which we used as initial conformations for additional MD simulations in GROMACS (lasting 0.1 ns), performed as described above (with pressure and temperature coupling). This generated, for each pressure, a set of 100 potential initial trajectories, starting from the intermediate configurations and ending either as a wurtzite or as a rock salt structure. From these trajectories, we merged the two trajectories that were initially closest (having the most similar volume per atom), but ending in the different crystal structures. These two trajectories were merged by reversing the trajectory ending in the wurtzite conformation, and appending the trajectory ending in the rock salt conformation. This generated artificial trajectories, connecting the wurtzite and rock salt structures, which were subsequently used as initial trajectories for the rare event simulations. The initial trajectories are non-continuous but transform into physical trajectories after the first accepted MC moves, and evolve into the more likely region of path space from thereon. In the analysis, the first 100 generated trajectories are excluded.

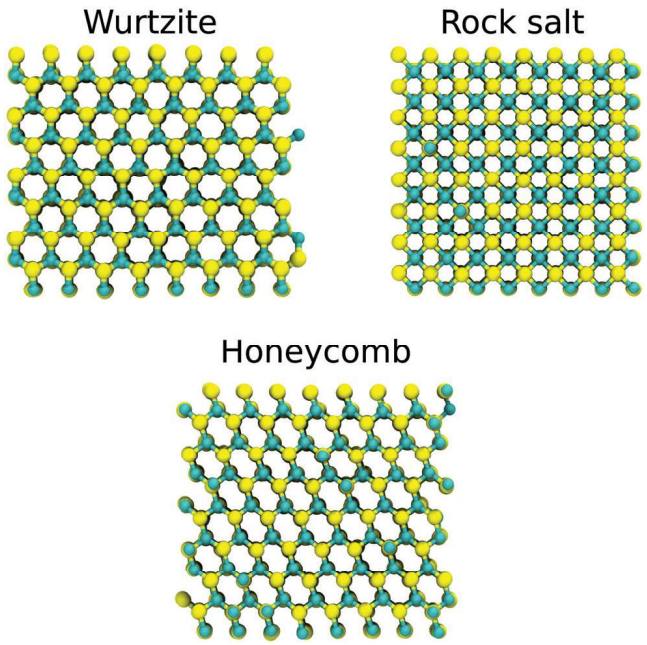

Fig. 1 Simulation snapshots showing the wurtzite and rock salt structures (10 GPa), and the 5-coordinated honeycomb structure (4 GPa). Cd (yellow) and Se atoms (cyan) are shown as spheres, and bonds between atoms are drawn using a cut-off of 3.4 Å.

2.2 Rare event simulations

To sample the transition between the wurtzite and rock salt structures, we carried out replica-exchange transition interface sampling (RETIS) simulations.[39] This is motivated by the low transition rate which prohibits brute-force MD simulations for obtaining rate constants. Further, this allows us to sample several reactive trajectories, without perturbing the dynamics, which in turn makes it possible to obtain statistics about possible reaction mechanisms.

The RETIS method uses an order parameter to describe the state of a (possibly) reactive trajectory. This order parameter, λ, defines two stable states, A and B, such that the system is in state A for $\lambda < \lambda_A$ and in state B for $\lambda > \lambda_B$, where λ_A and λ_B defines the boundaries for the two states, and $\lambda_A < \lambda_B$. In our case, we defined state A as the wurtzite structure and B as the rock salt structure. A simple order parameter that allows us to define the two stable states, and also satisfies $\lambda_A < \lambda_B$, is the negative volume per atom ($-V$) of the simulation box and this is the order parameter we have used for our RETIS simulations ($\lambda = -V$). For defining the stable states, we have made use of the equilibrium volumes per atom given in Table 1, however, since we are not guaranteed that the final configuration is a "perfect" rock salt structure, we have defined the final state B at a location that has a volume per atom larger than the rock salt volume per atom given in Table 1.

From the RETIS simulations, we calculate the rate constant, k_{AB}, for the transition as a product of a flux, f_A, and a crossing probability, $\mathscr{P}_A(\lambda_B|\lambda_A)$,

$$k_{AB} = f_A \times \mathscr{P}_A(\lambda_B|\lambda_A). \quad (1)$$

Table 1 Equilibrium volume per atom for CdSe structures at different pressures. The wurtzite structure is 4-coordinated, the honeycomb structure is 5-coordinated, and the rock salt structure is 6-coordinated

	Volume per atom (Å^3)		
Pressure (GPa)	Wurtzite	Honeycomb	Rock salt
11	—	—	21.049 ± 0.005
10	25.210 ± 0.014	—	21.242 ± 0.005
8	25.782 ± 0.012	—	21.667 ± 0.006
6	26.430 ± 0.010	—	22.162 ± 0.007
4	27.199 ± 0.009	26.24 ± 0.02	22.753 ± 0.008
2	28.157 ± 0.009	27.23 ± 0.02	23.490 ± 0.011

The initial flux measures the frequency for which potential reactive trajectories are initiated, and the crossing probability measures the probability of reaching state B, before (possibly) returning to the initial state A, given that the reaction was initiated by crossing the location λ_A. In our case, the crossing probability is a small number, which makes the determination of this quantity difficult in simulations. To deal with this problem, the RETIS method introduces several intermediate states λ_i such that $\lambda_0 = \lambda_A < \lambda_i < \lambda_B = \lambda_N$ and,

$$\mathscr{P}_A(\lambda_B|\lambda_A) = \prod_{i=1}^{N} \mathscr{P}_A(\lambda_i|\lambda_{i-1}), \quad (2)$$

which defines the small probability $\mathscr{P}_A(\lambda_B|\lambda_A)$ as a product of several larger probabilities $\mathscr{P}_A(\lambda_i|\lambda_{i-1})$, which measures the probability of reaching the (intermediate) location λ_i, before ending in state A or B, given that the trajectory initiated in state A and crossed λ_{i-1}. Further, the definition of the interfaces also defines the so-called path ensembles. In particular, the interface defined by λ_{N-1} defines the final path ensemble which samples the trajectories that typically reach furthest before returning to the initial state A, or ending in state B.

After having generated the initial artificial reactive trajectories (as described in Section 2.1), we started the main RETIS simulations. These simulations were carried out using PyRETIS[40,41] with GROMACS (with settings as described in Section 2.1) as the MD engine. In the RETIS simulations, we employed the shooting move with a frequency of 0.5 and the swapping move with a frequency of 0.5. The λ_i positions for the different pressures considered are given in Table S3 in the ESI.† The generated trajectories in the last path ensemble were extended for 40 ps with equilibrium MD simulations (settings as described in Section 2.1) to investigate if these trajectories indeed end in a rock salt-like structure, or return to a wurtzite-like structure. These extended trajectories were further analysed as described in Section 2.4.

2.3 Creation of defects

Starting from the wurtzite crystal structure consisting of 512 Cd and 512 Se atoms, we removed either 1, 2, 4, 8, or 16 pairs. The removal was carried out in either of two fashions:

- Uncorrelated random removal (Schottky defects): for the removal of n pairs, simply n Cd atoms and n Se atoms were randomly selected and removed. No correlation between Cd and Se removals was inflicted, nor between the Cd removals themselves or between the Se removals themselves. We will further refer to this approach as random removal.
- Cavity creation: For the removal of n pairs, we first randomly selected a single Cd atom. Then we removed this atom along with the $n - 1$ Cd atoms and the n Se atoms closest to it. We will further refer to this approach as cavity creation.

The resulting crystal either contains one single multi-site vacancy whenever the cavity creation was applied or many, up to $2n$, small vacancies. Occasionally the random removal could remove neighboring sites. These structures were not eliminated, but their effect is small due to their low probability of occurrence.

For each pressure (2, 4, 6, 8, and 10 GPa) we generated initial conformations with defects as described above. These initial conformations were then studied with plain MD simulations. We first energy minimized the conformations using a steepest descent algorithm, followed by a short (1 ns) *NVT* simulation (settings as described in Section 2.1, but without pressure coupling). We then carried out *NPT* simulations (settings as described in Section 2.1) lasting for 10 ns. The volume per atom was monitored during these MD simulations and used to assess the stability of the structures. After this, we studied the defects created by removing 16 pairs for 6, 8, and 10 GPa in more detail. For the two higher pressures we repeated the creation of defects 105 times (with subsequent MD simulations) before we studied the pressure of 6 GPa in a RETIS simulation.

It should be noted that while the force field[24] has been developed to realistically describe the different crystalline phases and has been used to describe different shapes and curvatures of nanoparticle surfaces, the inclusion of defects is yet unknown territory. The accuracy of the force field for these systems is, therefore, a somewhat open question. In particular, the random removal could be a source of concern as the local removal of individual atoms, more than local removals of Cd–Se pairs, could create local charges in the system that are not well accounted for in the Rabani force field employed in this study. With the advance of machine learning potentials,[42–44] these issues might be solved in the future. To address the quality of the force field used in this work, we have compared the stability of the different phases calculated with the Rabani force field to DFT calculations in Table S1 in the ESI.† Qualitatively, we get good agreement between the classical force field and the DFT calculations, and both methods agree on the relative stability of the different phases. To assess the accuracy when defects are included, we have compared defect energies calculated with the Rabani force field to defect energies calculated with DFT (see Table S2 in the ESI†). We generally find that the defect energies are overestimated (~20% higher when removing a single Cd–Se pair, and ~50% higher when removing 16 Cd–Se pairs) for the classical force field, but that the classical force field reproduces trends and the relative stability of different structures.

2.4 Analysis methods

After having obtained possibly reactive trajectories with the RETIS simulations, and extended them (starting from the

initial and last point of the RETIS-generated trajectories), we subjected these trajectories to further analysis: we calculated coordination numbers and Steinhardt order parameters[45] of order 3, 4, 5, and 6. We carried out the same analysis for the trajectories generated with plain MD simulations.

The coordination numbers were obtained by counting the number of neighbors for each atom within a distance of 3.4 Å (this cut-off was selected to include the first coordination shell, based on the equilibrium radial distribution functions for Cd–Se atoms). The same cut-off was also used for obtaining the Steinhardt order parameters.

3 Results

3.1 Equilibrium simulations

The volume per atom (used to define the stable wurtzite and rock salt states) is given in Table 1 as a function of the pressure, together with the volume per atom of the honeycomb structure in stable conditions. The obtained radial distribution functions are given in Fig. S1 in the ESI.†

To approximately investigate the stability region of the honeycomb structure we carried out MD simulations in the pressure range between 4 GPa and 6 GPa, in steps of 0.01 GPa. The number of atoms in different coordination numbers for these simulations can be found in Fig. S2 in the ESI,† and we find, approximately, that the honeycomb structure is (meta)-stable for pressures lower than 5.3 GPa.

3.2 Rare event simulations

The crossing probabilities and rate constants, as a function of the pressure, are given in Table 2. The number of interfaces required to climb the very steep barrier ranged from 10 for 10 GPa up to 30 for 2 GPa. Despite the small increments in the order parameter, some of the $\mathscr{P}_A(\lambda_i|\lambda_{i-1})$ were still very small (in the range 0.001–0.01). In addition, the shooting move had a rather low acceptance rate (1%). This gave rise to a rather large statistical uncertainty that is estimated to be in the order of two orders of magnitude.

The reason for this low acceptance is that the free energy *versus* the volume parameter is initially very steeply increasing. As a result, some of the RETIS path ensembles typically contain paths with only a few points above the ensemble's interface. Shooting from these points gives a reasonable chance to generate an accepted path, while shooting from other points leads to failed trajectories that do not cross the ensemble's interface.

Table 2 Crossing probabilities ($\mathscr{P}_A(\lambda_B|\lambda_A)$) and rate constants ($k_{AB}$) for the wurtzite to rock salt transition. Due to the small crossing probability and slow convergence, block averaging errors were unreliable, though the statistical errors are estimated to be in the range of 2 orders of magnitude

Pressure (GPa)	$\mathscr{P}_A(\lambda_B\|\lambda_A)$	k_{AB} (s^{-1})
10	1×10^{-5}	3×10^{5}
8	7×10^{-9}	5×10^{1}
6	1×10^{-16}	5×10^{-7}
4	2×10^{-28}	1×10^{-8}
2	1×10^{-34}	2×10^{-23}

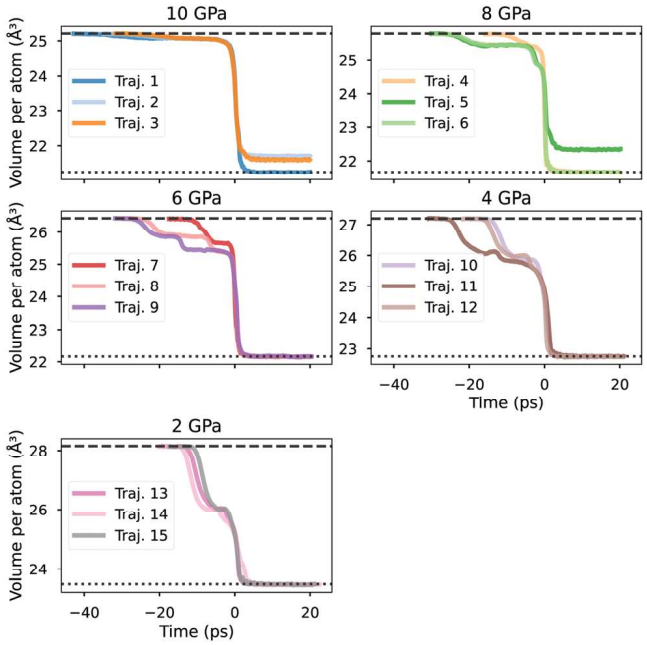

Fig. 2 Comparison of volume per atom for representative reactive trajectories at the considered pressures. The trajectories have been shifted in time so that the mean volume occurs at a time equal to 0 ps. For each pressure, we show three representative trajectories, which have been numbered consecutively. The horizontal lines show the volume per atom for the wurtzite (dashed line) and the rock salt structure (dotted line) at the different pressures.

Reducing the shooting range would be a way to increase the acceptance, though comes with a cost that sequential accepted trajectories will be highly correlated. Yet, a lot of sampling efficiency is probably to be gained from the newly developed MC moves,[46] which we plan to utilize for a future study on this topic.

Despite the large statistical uncertainty, a clear trend is still visible showing that both the crossing probability and rate constants go down by approximately 2–5 orders of magnitude per 1 GPa decrease, with the largest decrease happening at the lower pressures.

The change in the volume per atom for representative trajectories are shown in Fig. 2 for different pressure conditions. Here, we see that in some cases, at higher pressures (10 GPa and 8 GPa), the final structures have a volume per atom larger than the volume per atom of a pure rock salt structure. This is caused by a substantial amount of atoms that end up being 5-coordinated, rather than 6-coordinated, in the final structure as can be seen from the corresponding atomic coordination for the considered trajectories in Fig. 3. At lower pressures, the final state is closer to a fully formed rock salt structure.

We further noticed that for all pressures, a fully 5-coordinated state can occur. The emergence and existence of this state correlate with a kink in the volume *versus* time plots of Fig. 2. The 5-coordinated honeycomb structure or h-MgO was first predicted by Schön and Jansen[47] as a high energy polytype of NaCl, and later identified as a metastable intermediate for

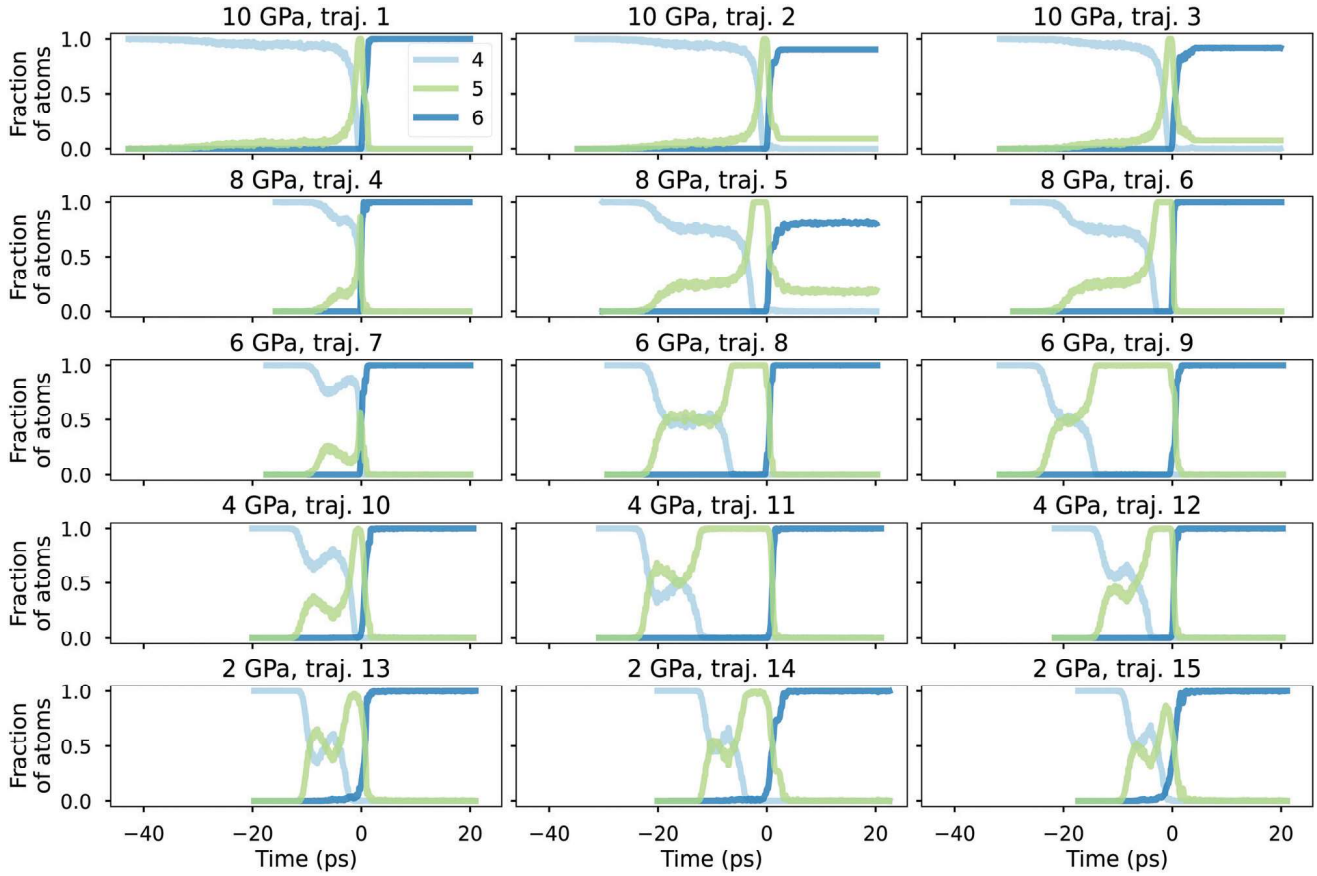

Fig. 3 Fraction of atoms assigned as 4-, 5-, or 6-coordinated for representative trajectories at the considered pressures. The time has been shifted identical to Fig. 2. The considered trajectories are the same as shown for the volume, and they are labeled with identical numbers.

the wurtzite to rock salt transition in MgO.[48] For CdSe, this intermediate has not yet been observed in experiments, and computational and theoretical studies do not fully agree on whether it is an important intermediate for the wurtzite to rock salt transition or not. Shimojo *et al.* did detect these structures in the MD simulations and analyzed them with DFT.[16] They concluded that the honeycomb structure was stable up to 4 GPa based on the DFT results. This is in agreement with metadynamics simulations that suggest that the wurtzite to rock salt transition has the honeycomb structure as an intermediate a low pressures ($\lesssim$2.5 GPa), but not at the higher pressures.[19] Still, TPS simulations at 2.5 GPa, which should reflect the actual dynamics more accurately, suggest that the mechanism through the 5-coordinate intermediate is unfavorable.[17,19]

The lifetime of this fully 5-coordinated state in transition trajectories seems largest at the intermediate pressures (4 and 6 GPa) where it can exist up to 150 ps (see trajectory 18 at 6 GPa in Fig. S7 in the ESI†). At the lower pressure of 2 GPa, this state also emerges as an intermediate though with a shorter lifetime, while it is even shorter at 8 and 10 GPa.

The apparent longer lifetime at 4 and 6 GPa trajectories seems to indicate that the long-lived 5-coordinated state at these pressures is a metastable intermediate that can be avoided at lower pressures whenever the system is less forcefully pushed over the barrier. Indeed, if we inspect the mean Steinhardt order parameters q_4 and q_6 of Fig. S3 of the ESI,† we see that the fully 5-coordinated states of 2 GPa differ from those at 4 and 6 GPa. When we consider the time interval of the fully 5-fold coordinated state, we see that the q_6 parameter is lower at 2 GPa then at 4 and 6 GPa, while the reverse is true for the q_4 parameter. This indicates that these structures are not identical and that the 2 GPa 5-fold coordinated structure is not acting as a long-lived temporary trap, like it is for the 4 and 6 GPa cases, that prevents an immediate transition to the 6-coordinated state.

The n-fold coordinated state does not necessarily correlate with a large q_n Steinhardt parameter.[49] A clear correlation can, however, be found between the q_5 parameter, the 5-fold coordination, and an intermediate plateau in the volume *versus* time curve (see Fig. S4–S10 of the ESI†). The point where the system is fully 5-coordinated coincides with a local maximum in the q_5 curve. Remarkably, the maximum in the q_5 parameter is the highest for the low pressures while it remains at a lower plateau for the 4 and 6 GPa cases that have been trapped in this intermediate. Moreover, at the end of the plateau, we can observe a sudden increase followed by an immediate decrease to nearly zero. This is especially clear for trajectory 18 at 6 GPa that has a very long lifetime in the 5-coordinated state. This shows that a 5-fold coordinated state with a low q_5 parameter is indicative of the intermediate acting as a long-lived trap, while

a high q_5 value reflects that the transition bypasses the trap or escapes from it.

So where this 5-coordinated metastable state is avoided at low pressures, at the higher pressures (8 and 10 GPa) any 5-coordinated state simply becomes too unstable (see Fig. S7 of the ESI†). Hence, the probability to get trapped for a long time in the fully 5-coordinated structure is the highest at the intermediate pressures when considering wurtzite to rock salt transitions. This could explain why the honeycomb structure was not observed[17] in TPS at 2.5 GPa. Even if the structure is relatively stable and would trap the system for a relatively long time if it would be accessed, the dynamical route at low pressures seems to bypass this trap, unlike the artificial dynamics of the metadynamics method.[19]

Inspecting the changes of the individual simulation box parameters (see Fig. S15 and S16 of the ESI†) also points towards there being a difference the transition dynamics at low and high pressures. For the higher pressures, we find that two of the box vectors expand, while the third one is contracting. When this happens, Cd and Se atoms move into the same layer (as they are in the intermediate honeycomb structure). This can also be seen from visual inspection of the trajectories (see the accompanying movies of representative trajectories in the ESI†). After the intermediate structure is formed, all three box vectors contract, and this forms the rock salt structure. At pressures of 8 and 6 GPa, we observe regions where the box parameters stay approximately constant (after forming the intermediate structure), before the final contraction into to rock salt structure. At the higher pressure (10 GPa) this is much less pronounced (the change appears more continuous) while at the lower pressures (2 and 4 GPa) there are no such regions. And in fact, for the lowest pressures, we observe cases where all box vectors are contracting throughout the transformation.

3.3 Effect of defects

The final volume obtained after 10 ns of the MD simulations with defects made by random removal and cavity creation are shown as a function of pressure in Fig. 4.

At 10 GPa, the introduction of defects leads to a spontaneous transition in all cases, while for the lower pressures (2, 4, and 6 GPa) the introduction of the defects do not induce transitions to a rock salt structure within 10 ns. At 8 GPa we find that removal of 16 or 8 pairs leads to a transition in the MD runs after removing the pairs with the random removal approach. With the cavity creation approach at the same pressure, only the removal of 16 pairs lead to a transition. Structures with fewer defects remain in the wurtzite structure. At 6 GPa none of the cases lead to a transition, and we studied the random removal of 16 pairs at this pressure in more detail with a RETIS simulation. We report on this RETIS simulation after first discussing additional MD results for the higher pressures.

We defined the first passage time for the transition as the point in time (measuring from the start of the *NPT* simulation) where the volume first reaches 98% of its final volume. The first passage times are shown in Fig. 5. At 10 GPa the mean first passage times are 3.7 ps (random removal) and 4.4 ps (cavity creation), while the mean first passage times are 8 ps (random removal) and 11 ps (cavity creation) at 8 GPa. We carried out a one-way analysis of variance to investigate if the two different ways of introducing defects lead to different mean first passage times. We found that the mean first passage times are statistically different (see Table S4 in the ESI†) for random removal and cavity creation, both at 10 and 8 GPa, and that the random removal results in shorter transition times. The difference in mean first passage times between random removal and cavity creation increases when the pressure decreases as can be concluded from Fig. 5 and from the fact that the removal of 8 pairs at 8 GPa only lead to a transition for the random removal.

At 6 GPa none of the MD simulations showed a spontaneous transition within the 10 ns time interval. However, to study the effect of pair removal at this pressure, we performed one additional RETIS simulation in which 16 pairs were randomly removed. The RETIS simulation showed a crossing probability equal to 10^{-12} and a rate constant equal to 50 s^{-1}. This is compared to the rate constants at 10 and 8 GPa (with the same number of pairs removed) in Table 3. For all pressures, the

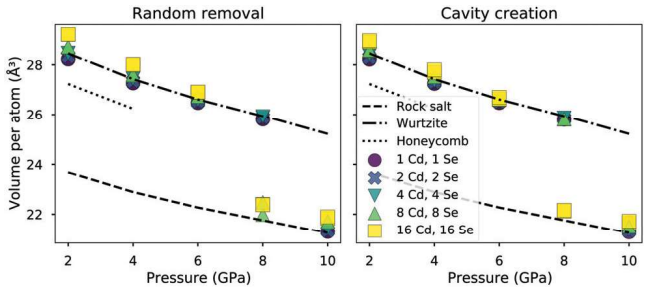

Fig. 4 The final volume per atom obtained after 10 ns of MD simulations, starting from wurtzite structures with defects. The labels indicate the number of atoms removed when generating the defects. Each case (including the generation of defects) was repeated twice. The lines show the volume per atom for the wurtzite structure (dash-dotted line), the honeycomb structure (dotted line), and the rock salt structure (dashed line).

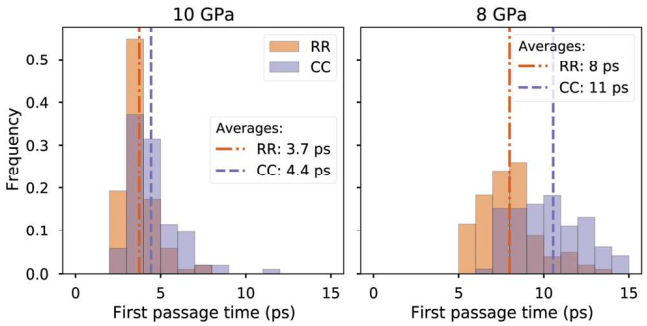

Fig. 5 The first passage times for transitions from the structures with defects (created by removing 16 pairs from the wurtzite structures) to rock salt structures at 10 and 8 GPa. The label "RR" represents defects introduced by random removal, and "CC" represents defects introduced by cavity creation. Each case (including the generation of defects) was repeated 105 times. The vertical lines show the mean first passage times for the random removal (dash-dotted line) and the cavity creation (dashed line).

Table 3 Rate constants (k_{AB}) for the wurtzite to rock salt transition with defects created by removing 16 pairs. Here, we abbreviate the random removal as "RR" and cavity creation as "CC". The rate constants for the cases at 10 and 8 GPa were estimated from the mean first passage times, and the rate constant at 6 GPa was calculated with a RETIS simulation

Pressure (GPa)	Defect type	k_{AB} (s^{-1})
10	RR	2.7×10^{11}
10	CC	2.3×10^{11}
8	RR	1.3×10^{11}
8	CC	9.1×10^{10}
6	RR	5.0×10^{1}

introduction of defects increases the rate constant significantly (compared to the cases with no defects), but the transition at 6 GPa is still relatively slow, which is consistent with the fact that no transition was observed in the 10 ns MD run. Nevertheless, the rate at 6 GPa increases due to defects by 8 orders of magnitude and is comparable to the rate constant at 8 GPa for the case without defects.

In Fig. S11–S14 (ESI†) we show the coordination numbers and Steinhardt order parameters for representative trajectories from the simulations of the systems with defects. In contrast to the system without defects, we never observe the long-lived 5-coordinated intermediate. This can also be seen in the evolution of the simulation box parameters (see Fig. S17 of the ESI†), where no intermediate plateaus are observed. The absence of this intermediate was also reported by Grünwald *et al.*[7] for spherical CdSe nanocrystals. The spherical geometry is not fully commensurate with the crystal lattice which leads to disordered surfaces or stacking faults.[9] Hence, these can have a similar effect as bulk defects. Our results, showing that defects cause a huge increase in the transition rate, also support the general belief that solid–solid transformations predominantly nucleate at lattice defects,[9,50] which would explain why the h-MgO structure is not observed in experiments.

4 Conclusions

The transition from wurtzite to rock salt in CdSe was studied using molecular dynamics and path sampling techniques (RETIS). We investigated the transition for structures without defects and for structures with defects at pressures ranging from 2 to 10 GPa.

The bulk structures without defects exhibit a transition *via* a honeycomb-like structure where the atoms are 5-coordinated. The longest lifetime for this structure along the transition paths is obtained for the intermediate pressures of 4 and 6 GPa. We note that a short lifetime observed in transition paths is not necessarily related to a thermodynamically short lifetime, since the configurations along transition paths do not follow the equilibrium distribution. The transitions at 2 GPa suggest that the natural dynamics of the wurtzite to rock salt transition can bypass the long-lived metastable state, but briefly visits another 5-coordinated state. This short-lived 5-coordinated state (that does not trap the system) differs from the long-lived 5-coordinated structures observed at 4 and 6 GPa, as can be concluded from the Steinhardt order parameters. In particular, the q_5 order parameter is an indicator of this difference. For all transitions, when passing through a fully 5-coordinated state, the q_5 parameter has a local maximum. This maximum is higher for the transitions that do not get trapped. In addition, for q_5 we see a sudden increase, followed by a sharp decrease, when the system is able to escape from the 5-coordinated trap. This very short lifetime at 2 GPa can explain why earlier TPS[17] simulations did not identify the honeycomb structure as an important intermediate at 2.5 GPa. In contrast, the intermediate was observed at low pressures in metadynamics simulations,[19] which reflects the thermodynamic stability of this state. Since metadynamics utilizes a the time-dependent biasing potential to enforce the transition, the trajectories are not representing the Newtonian equation of motion. Apparently, this artificial dynamics is more likely to get trapped in the long-lived 5-coordinated state than the natural dynamics of the system. At the high pressures (8 GPa and 10 GPa), the 5-coordinated state becomes unstable and is only observed for a few ps during the transition process. Still, its effect can remain since the final structures of the 8 GPa and 10 GPa transitions are sometimes imperfect rock salt crystals in which some atoms remain 5-fold coordinated.

The rate of transition increased by several orders of magnitude for the CdSe structures with defects at 6–10 GPa. At 10 GPa, all wurtzite structures with defects transformed spontaneously within 10 ns. The rate was higher for the structures where Cd and Se atoms were removed randomly, compared to when the defects were introduced in clusters (by the cavity creation). We note that this might be caused by a larger local charge imbalance, created when the atoms are removed randomly.

The 5-coordinated structure is not found in experiments, and in our simulations with defects, we also do not find a long-lived 5-coordinated intermediate. This correspondence, and the large increase in the transition rate for systems with defects, supports the notion that a solid–solid transformation predominantly occurs at lattice defects that serve as nucleation centers.

Conflicts of interest

There are no conflicts to declare.

Acknowledgements

The computer simulations were performed on resources provided by UNINETT Sigma2 – the National Infrastructure for High Performance Computing and Data Storage in Norway, project numbers NN9355k and NN9718k. Q3

Notes and references

1 I. Robel, V. Subramanian, M. Kuno and P. Kamat, *J. Am. Chem. Soc.*, 2006, **128**, 2385–2393.

2 V. Colvin, M. Schlamp and A. Alivisatos, *Nature*, 1994, **370**, 354–357.
3 W. Chan and S. Nie, *Science*, 1998, **281**, 2016–2018.
4 M. P. Lima, L. Cabral, E. Margapoti, S. Mahapatra, J. L. F. Da Silva, F. Hartmann, S. Höfling, G. E. Marques and V. Lopez-Richard, *Phys. Rev. B*, 2019, **99**, 014424.
5 B. Kong, X.-Y. An, T.-X. Zeng and J. Zhang, *Phys. Chem. Chem. Phys.*, 2020, **22**, 7474–7482.
6 A. Mannodi-Kanakkithodi, M. Y. Toriyama, F. G. Sen, M. J. Davis, R. F. Klie and M. K. Y. Chan, *npj Comput. Mater.*, 2020, **6**, 39.
7 M. Grünwald, E. Rabani and C. Dellago, *Phys. Rev. Lett.*, 2006, **96**, 255701.
8 M. Grünwald, C. Dellago and P. L. Geissler, *J. Chem. Phys.*, 2007, **127**, 154718.
9 M. Grünwald and C. Dellago, *Nano Lett.*, 2009, **9**, 2099–2102.
10 M. Grünwald and C. Dellago, *J. Chem. Phys.*, 2009, **131**, 164116.
11 B. Li, K. Bian, X. Zhou, P. Lu, S. Liu, I. Brener, M. Sinclair, T. Luk, H. Schunk, L. Alarid, P. G. Clem, Z. Wang and H. Fan, *Sci. Adv.*, 2017, **3**, e1602916.
12 T. Mandal, *Appl. Phys. Lett.*, 2012, **101**, 021906.
13 B. Fu, L. Chen, Y. Xie, Y. Feng and X. Ye, *J. Nanopart. Res.*, 2015, **17**, 354.
14 D. Sheppard, P. Xiao, W. Chemelewski, D. D. Johnson and G. Henkelman, *J. Chem. Phys.*, 2012, **136**, 074103.
15 P. Xiao, D. Sheppard, J. Rogal and G. Henkelman, *J. Chem. Phys.*, 2014, **140**, 174104.
16 F. Shimojo, S. Kodiyalam, I. Ebbsjö, R. K. Kalia, A. Nakano and P. Vashishta, *Phys. Rev. B: Condens. Matter Mater. Phys.*, 2004, **70**, 184111.
17 D. Zahn, Y. Grin and S. Leoni, *Phys. Rev. B: Condens. Matter Mater. Phys.*, 2005, **72**, 064110.
18 C. Bealing, R. Martoňák and C. Molteni, *J. Chem. Phys.*, 2009, **130**, 124712.
19 C. Bealing, R. Martoňák and C. Molteni, *Solid State Sci.*, 2010, **12**, 157–162.
20 S. Leoni, R. Ramlau, K. Meier, M. Schmidt and U. Schwarz, *Proc. Natl. Acad. Sci. U. S. A.*, 2008, **105**, 19612–19616.
21 L. Zhu, R. E. Cohen and T. A. Strobel, *J. Phys. Chem. Lett.*, 2019, **10**, 5019–5026.
Q4 22 A. Mariano and E. Warekois, *Science*, 1963, **142**, 672–&.
23 J. N. Wickham, A. B. Herhold and A. P. Alivisatos, *Phys. Rev. Lett.*, 2000, **84**, 923–926.
24 E. Rabani, *J. Chem. Phys.*, 2002, **116**, 258–262.
25 A. Laio and M. Parrinello, *Proc. Natl. Acad. Sci. U. S. A.*, 2002, **99**, 12562.
26 C. Dellago, P. G. Bolhuis, F. S. Csajka and D. Chandler, *J. Chem. Phys.*, 1998, **108**, 1964.
27 B. Peters, G. T. Beckham and B. L. Trout, *J. Chem. Phys.*, 2007, **127**, 034109.
28 T. S. van Erp, D. Moroni and P. G. Bolhuis, *J. Chem. Phys.*, 2003, **118**, 7762–7774.
29 T. S. van Erp, *Phys. Rev. Lett.*, 2007, **98**, 268301.
30 T. S. van Erp, M. Moqadam, E. Riccardi and A. Lervik, *J. Chem. Theory Comput.*, 2016, **12**, 5398.
31 M. Moqadam, A. Lervik, E. Riccardi, V. Venkatraman, B. K. Alsberg and T. S. van Erp, *Proc. Natl. Acad. Sci. U. S. A.*, 2018, **115**, E4569–E4576.
32 S. Roet, C. D. Daub and E. Riccardi, *J. Chem. Theory Comput.*, 2021, **17**, 6193–6202.
33 M. J. Abraham, T. Murtola, R. Schulz, S. Páll, J. C. Smith, B. Hess and E. Lindahl, *SoftwareX*, 2015, **1–2**, 19–25.
34 U. Essmann, L. Perera, M. L. Berkowitz, T. Darden, H. Lee and L. G. Pedersen, *J. Chem. Phys.*, 1995, **103**, 8577–8593.
35 G. Bussi, D. Donadio and M. Parrinello, *J. Chem. Phys.*, 2007, **126**, 014101.
36 M. Bernetti and G. Bussi, *J. Chem. Phys.*, 2020, **153**, 114107.
37 M. Parrinello and A. Rahman, *J. Appl. Phys.*, 1981, **52**, 7182–7190.
38 S. Plimpton, *J. Comput. Phys.*, 1995, **117**, 1–19.
39 T. S. van Erp, *Phys. Rev. Lett.*, 2007, **98**, 268301.
40 A. Lervik, E. Riccardi and T. S. van Erp, *J. Comput. Chem.*, 2017, **38**, 2439–2451.
41 E. Riccardi, A. Lervik, S. Roet, O. Aarøen and T. S. van Erp, *J. Comput. Chem.*, 2020, **41**, 370–377.
42 J. Behler and M. Parrinello, *Phys. Rev. Lett.*, 2007, **98**, 146401.
43 J. S. Smith, O. Isayev and A. E. Roitberg, *Chem. Sci.*, 2017, **8**, 3192–3203.
44 J. Vandermause, S. B. Torrisi, S. Batzner, Y. Xie, L. Sun, A. M. Kolpak and B. Kozinsky, *npj Comput. Mater.*, 2020, **6**, 20.
45 P. J. Steinhardt, D. R. Nelson and M. Ronchetti, *Phys. Rev. B: Condens. Matter Mater. Phys.*, 1983, **28**, 784–805.
46 E. Riccardi, O. Dahlen and T. S. van Erp, *J. Phys. Chem. Lett.*, 2017, **8**, 4456–4460.
47 J. Schon and M. Jansen, *Angew. Chem., Int. Ed. Engl.*, 1996, **35**, 1287–1304.
48 S. Limpijumnong and W. Lambrecht, *Phys. Rev. B: Condens. Matter Mater. Phys.*, 2001, **63**, 104103.
49 W. Mickel, S. C. Kapfer, G. E. Schroeder-Turk and K. Mecke, *J. Chem. Phys.*, 2013, **138**, 044501.
50 J. M. Besson, J. P. Itié, A. Polian, G. Weill, J. L. Mansot and J. Gonzalez, *Phys. Rev. B: Condens. Matter Mater. Phys.*, 1991, **44**, 4214–4234.